Effects of the Temperature on the Hydrogen Permeation Behaviours of L360NCS Pipeline Steel in 1MPa H$_2$S Environments

Shuqi Zheng[*], *Chengshuang Zhou, pengyan Wang, Changfeng Chen, and Liqiang Chen*

State Key Laboratory of Heavy Oil Processing and Department of Materials Science and Engineering, China University of Petroleum, Beijing 102249, China
[*]E-mail: zhengsq09@163.com

High-temperature and high-pressure electrochemical measurement techniques, scanning electron microscopy and X-ray diffraction were applied to investigate the effects of the corrosion product films formed on the surface of L360NCS pipeline steel at different temperatures on the hydrogen permeation and the corrosion rate in high pressure H$_2$S environments. The results indicate that hydrogen permeation occurs in three stages: rising stage, declining stage and steady stage. The peak values of hydrogen permeation curves increased with increasing temperature, but the total hydrogen permeation flux before the steady stage decreased with increasing temperature. The characteristics of the total hydrogen permeation flux are similar to that of the average corrosion rates. The hydrogen permeation currents are highly dependent on the transformation of the crystal structures of the corrosion product films, which were converted from a mixture of troilite and mackinawite at 25 °C to a mixture of mackinawite and pyrrhotite at 80 °C.

Keywords: Pipeline steel, Hydrogen permeation, Corrosion rate, Corrosion product film.

1. INTRODUCTION

H$_2$S is a very dangerous corrosion agent in petroleum plants due to its role in the corrosion process, which generates H atoms that may penetrate into the steel surface and originate many cracks and fractures in steel used in industrial equipment. The complex work conditions of high temperature, high pressure and multiphase flows accelerate the corrosion of pipeline steel in H$_2$S environments [1].

Hydrogen embrittlement of steel can lead to steel corrosion at room temperature but also at high temperatures (blue brittleness temperatures) [2, 3]. However, some studies [4, 5] suggested that the effects of hydrogen on pipeline steel corrosion were small at high temperatures due to the rapid

diffusion and desorption rate of hydrogen and that no significant hydrogen atmosphere could form either at the dislocations or at the slip barriers. The solubility of hydrogen sulphide in aqueous solutions containing strong electrolytes increases with an increase in the H_2S partial pressure, but the solubility decreases with an increase of temperature [6]. The structures of the corrosion product films formed on carbon steel immersed in a solution containing hydrogen sulphide depended on the temperature and the solubility of hydrogen sulphide [7-9]. Furthermore, the corrosion products can promote or inhibit the iron corrosion, resulting in the formation of a ferrous sulphide (FeS) protective film on the metal surface [10,11]. Thus, the effects of corrosion films at different temperatures on the hydrogen embrittlement are very complicated. Hydrogen permeation through a metallic membrane by an electrochemical technique is a common method for studying hydrogen diffusivity and metallic embrittlement phenomena [12-17]. Therefore, the hydrogen permeation test and the corrosion rate measurement are used to study the protection properties of the corrosion films in high partial pressure H_2S environments.

The goal of the present investigation is to understand the effects of the corrosion films on the hydrogen permeation and corrosion rates of L360NCS pipeline steels. To achieve this objective, a high-temperature and high-pressure electrochemical permeation cell was developed. The hydrogen permeation current was measured in wet high-pressure H_2S environments at different temperatures. The corrosion rates and the permeation currents were measured simultaneously. The corrosion products were characterised using scanning electron microscopy (SEM) and X-ray diffraction (XRD).

2. EXPERIMENTAL PROCEDURES

2.1 Tested material

These specimens were obtained from commercial products of L360NCS grade pipeline steel. The specimens used for the permeation experiments were 25-mm diameter plates with a thickness of 3 mm. All the faces of the plates were polished using 1200-grit silicon carbide paper. Specimens for the weight loss tests (sized 50 mm × 10 mm × 3 mm) were pre-treated in a manner that was similar to the permeation specimens. The specimens used for measuring hydrogen diffusivity by the means of electrochemical charge were 25-mm diameter plates with a thickness of 2 mm. The surfaces of these specimens were finished in the same manner as the permeation specimens.

2.2 Test solutions and exposure conditions

To clarify the effects of the corrosion product films on hydrogen permeation behaviour, the tests were performed in 5% NaCl solution without acetic acid to avoid the introduction of additional hydrogen ions. In this test, the corrosion product films were deposited at different temperatures: 25 °C, 35 °C, 50 °C and 80 °C. The H_2S pressure was 1.0 MPa.

2.3 Electrochemical hydrogen permeation test

To investigate the effects of the corrosion product films formed at high temperature and high pressure environments on hydrogen permeation, a high-temperature and high-pressure hydrogen permeation device was designed and manufactured. A sketch of the experimental equipment was described in reference[18]. In this device, the test specimen seals the high-temperature and high-pressure chamber, which can be used in an environment with pressure of over 2 MPa and temperature of over 250 °C. In the cathodic side, the cell is filled with test solutions containing H_2S at a pressure of 1 MPa, and a potential is not applied. However, the detection side is filled with a 0.2 N NaOH solution, and an overvoltage of 0 mV_{SCE} is applied to oxidise the diffused hydrogen. The detection side of the steel membrane was electroplated with palladium to eliminate flux-limiting surface impedances and to ensure the reliability of the hydrogen oxidation current. The thickness of the specimens is 3 mm. The hydrogen permeation rate was determined from the hydrogen oxidation current density.

As the goal of the paper is to investigate the effect of H_2S on the permeation of hydrogen in pipeline steels at different temperatures, hydrogen is introduced into the samples by corrosion reaction of H_2S and iron instead of electrochemical charging. Thus, it is necessary to describe the permeation test procedures in detail. First, the specimen was clipped into the device. Next, the de-aerated 5% NaCl and the de-aerated 0.2 N NaOH were selected as test solutions in the hydrogen charging cell and the hydrogen oxidation cell, respectively. To ensure the continuous de-aeration of the NaOH solution and NaCl solution in the passivated medium, N_2 gas was bubbled through the solution for 2 hours at a flow rate of 10 ml min^{-1} per litre of solution. After the bubbled N_2 gas flow, the temperature was increased to the desired value. Then, the potential of the steel membrane on the hydrogen oxidation cell was maintained at a potential of 0 mV_{SCE}, at which the dominant oxidation reaction was the oxidation of hydrogen that diffused through the steel membrane. After 24 hours of passivation, the background current was stabilised and remained lower than 2×10^{-6} A (because the hydrogen charging cell was made of metal, the background current was often higher than that from a cell made of an insulator, whose background current can often be lower than 0.5×10^{-6} A), the H_2S gas was continuously bubbled through the 5% NaCl solution and maintained a requirement of a partial pressure of 1.0 MPa and a controlled flow rate of 10 ml min^{-1} per litre of solution to ensure fresh H_2S gas. The hydrogen oxidation current was continuously measured.

The apparent hydrogen diffusivity at different temperatures in steels can be determined using the breakthrough time method or the relaxation time method. In this study, the relaxation time method was used to determine the hydrogen diffusivity for the tested steels.

2.4 Corrosion rates test

Standard weight loss tests were also performed using the ASTM G31 procedure. The standard weight loss tests were performed in the hydrogen-generating cell of the high-temperature and high-pressure hydrogen permeation device. After the specimens for the weight loss tests were weighed, they were immersed into the test medium, as described in the section highlighting the test conditions. The corrosion time was consistent with the electrochemical hydrogen permeation test. After the corrosion

test, the specimens were removed from the medium. The corrosion scales were cleaned, and the specimens were dewatered and dried before they were weighed again. General corrosion rates were calculated based upon the weight loss of the samples.

3. RESULTS AND DISCUSSION

The samples used for this study were cut from L360NCS pipeline steel, which is widely used in sour oil and gas fields, with the chemical composition (wt%): C 0.13, Si 0.4, Mn 1.5, P 0.02, S 0.003, Cr 0.3, and Fe constituting the balance. The microstructure with ferrite (F) and pearlite (P) was described in reference [18].

3.1. Permeation experiments

Hydrogen permeation tests were performed to investigate the effect of environmental temperature on hydrogen diffusion, which is related to hydrogen damage. The typical hydrogen permeation curves measured for 3-mm steel membranes exposed to test environments composed of 5% NaCl solution with 1 MPa H_2S at different temperatures are shown in Fig. 1.
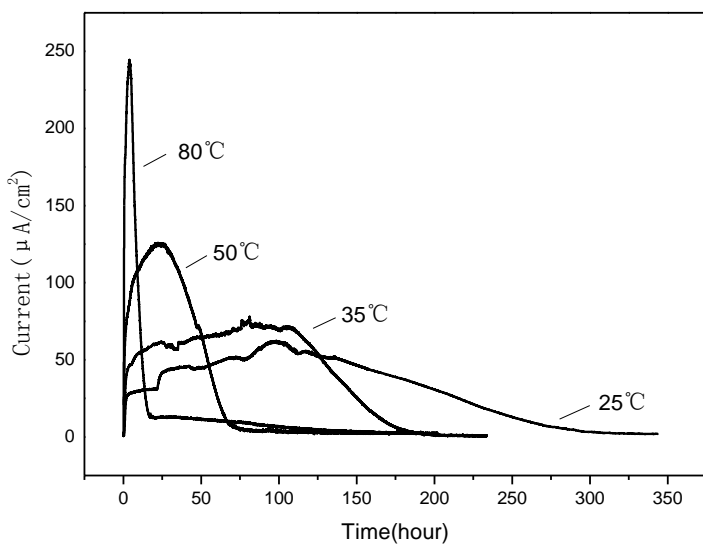
Figure 1. Hydrogen permeation curves measured for 3-mm steel membranes exposed to the test environments composed of 5% NaCl solution with 1 MPa H_2S at different temperatures.

The first important aspect to be outlined is the similarity between the hydrogen permeation curves. All of the hydrogen permeation curves exhibited three stages, consisting of a rising stage, declining stage and steady stage. Note that the peak values increased with increasing temperature and that the slopes of the curve change rapidly. The difference in the hydrogen permeation curves is thought to be closely dependent on the corrosion reaction at the steel surface. The hydrogen

permeation rate increases with the increase in the number of hydrogen atoms formed as a result of the corrosion reaction and penetration into the steel. When a corrosion product film is formed on the steel surface, it may suppress the corrosion reaction. The type of hydrogen permeation curves observed indicated that the corrosion product films that are formed in 5% NaCl with 1.0 MPa H_2S at varying temperatures inhibit the production of hydrogen atoms and the protection of corrosion product films became more obvious as the temperature increased from 25 °C to 80 °C.

To more clearly evaluate the temperature on the corrosion reaction, which much effect the hydrogen permeation curves, the parameters including hydrogen permeation flux, the summation of hydrogen permeation flux, and effective hydrogen diffusivity were analysed. The flux of hydrogen through the specimen was measured in terms of the steady-state current density, I_p (A/m^2), and was converted to the steady-state hydrogen permeation flux, J_∞ (mol/cm^{2}s), according to the following equation:

$$J_\infty = I_P^\infty / nF \qquad (1)$$

The hydrogen permeation rate Φ (mol/cm s) is defined as

$$\Phi = J_\infty L = L I_P^\infty / nF \qquad (2)$$

The total hydrogen permeation flux Σ_H is defined as

$$\sum H = \sum_{0 \to t_s} J \times \Delta t = \sum_{0 \to t_s} I_p \times \Delta t / nF \qquad (3)$$

where I_p^∞ is the steady-state permeation current density, n is the number of transferred electrons, F is the Faraday's constant, L (cm) is the specimen thickness, J_∞ is the steady-state flux, J is the instantaneous hydrogen permeation flux, Δt is the interval time and, t_s is the steady state time.

The effective hydrogen diffusivity, D_{eff} (cm^2/s), which is the rate-limiting step, is related to the time lag by

$$D_{eff} = L^2 / 6t_L \qquad (4)$$

where t_L (s) is the lag time, defined as 0.63 times the steady-state value, and D_{eff} is determined from the transient t_L. If the surface hydrogen was in thermodynamic equilibrium with the subsurface hydrogen, the apparent hydrogen solubility C_{app} (mol/cm^3) is defined by

$$C_{app} = J_\infty L / D_{eff} \qquad (5)$$

As the apparent hydrogen solubility is related to the hydrogen ion concentration in solution including 1.0 MPa H_2S, more work needs to be performed. The solubility of H_2S, K_{H2S}, at different temperatures is calculated by [19]

$$\ln K_{H_2S} = 5.0375 + 0.011280P - 2.0071 \times 10^{-5} \times P^2 + 1.5586 \times 10^{-8} \times P^3 - 0.044033T + 5.7530 \times 10^{-6} T^2 + 8.0270 \times 10^{-8} T^3 \qquad (6)$$

where is P is the partial pressure of H_2S (lb/in^2), T is in Kelvin. The hydrogen ion concentration $[H^+]$ is defined by

$$[H^+] = k_1 \times C_{H_2S} / [HS^-] \qquad (7)$$

where k_1 is the first ionisation constant and C_{H2S} is the solubility of H_2S.

To obtain the D_{eff} of hydrogen atoms in base metal at different temperatures, the permeation curves for the specimens at different temperatures were measured by the standard electrochemical permeation technique [20].
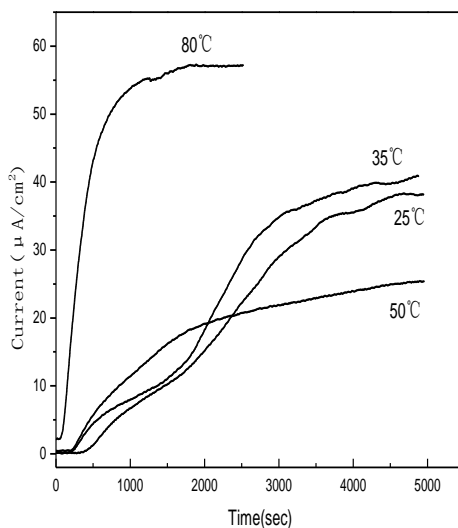
Figure 2. The permeation curves of hydrogen in the base metal at different temperatures measured by the standard electrochemical permeation technique.

Fig. 2 shows the permeation curves of hydrogen in the base metal at different temperatures measured by the standard electrochemical permeation technique. Note that the slope of the current increased with increasing temperature. We can use the results to calculate the diffusion coefficient by the time lag method with the mathematical expression derived from Fick's second law. In this investigation, the hydrogen diffusion coefficients, the peak values of hydrogen permeation rate, the peak values of the apparent hydrogen solubility, the solubility of H_2S, the hydrogen ion concentration

and the summation of hydrogen permeation flux at different temperatures defined by Eqs. (1)-(7) are shown in Fig. 3.
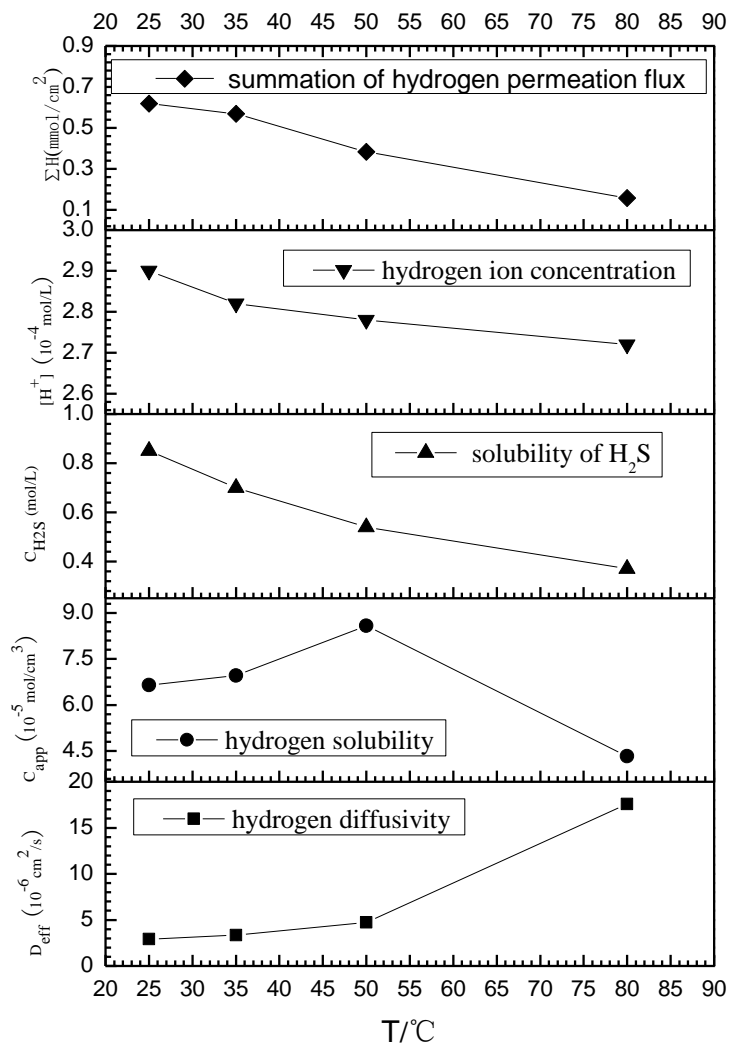
Figure 3. The hydrogen diffusion coefficients in the base metal, hydrogen solubility C_{app}, solubility of H2S C_{H2S}, the hydrogen ion concentration [H$^+$] and the total hydrogen permeation flux Σ_H at different temperatures.

The mean value of the hydrogen diffusivity increased from 2.92×10^{-6}, 3.33×10^{-6}, 4.57×10^{-6} to 17.57×10^{-6} cm^2/s when the test temperature increased from 25, 35, 50 to 80°C, respectively. The total hydrogen permeation flux before the steady stage or Σ_H were calculated from Eq. (3); it decreased from 0.62 mol/cm^2 at 25°C to 0.16 mol/cm^2 at 80°C. The values at 25°C and 35°C exhibited little change, but it decreased obviously when the temperature increased to 50°C. The peak values of hydrogen solubility of the specimens studied in the high-temperature and high-pressure hydrogen permeation device with 1.0 MPa H2S or C_{app} were calculated from Eq. (5) and appeared to increase with increasing temperature; C_{app} increased to a maximum value of 8.58×10^{-5} mol/cm^3 at 50°C in the limited data points obtained. After 50°C, the C_{app} declined with increasing of temperature. The C_{app} decrease

indicates that the corrosion product films require less time to perform protective properties at a higher temperature. As the salting-out effect of NaCl on H_2S solubility is nearly independent of temperature below 100°C [21], the solubility of H_2S or C_{H2S} that was calculated from Eq. (6) appeared to decrease with increasing temperature. As the first ionisation constant for H_2S decreased from 7.0 at 25°C to 6.7 at 80°C [22], the hydrogen ion concentration or $[H^+]$ at different temperatures can be calculated from Eq. (7); the calculated results indicated that the $[H^+]$ decreased from 2.90×10^{-4} at 25°C to 2.72×10^{-4} at 80°C. However, the $[H^+]$ did not change significantly, with only a decrease of approximately 5%.

The results of the hydrogen permeation curves and the values of the solubility suggest that the temperature performed a significant effect on the behaviour of hydrogen permeation, as the $[H^+]$ did not change significantly. The peak value of C_{app} decreasing significantly at 80°C was considered to be due to effective protection by the corrosion product film.
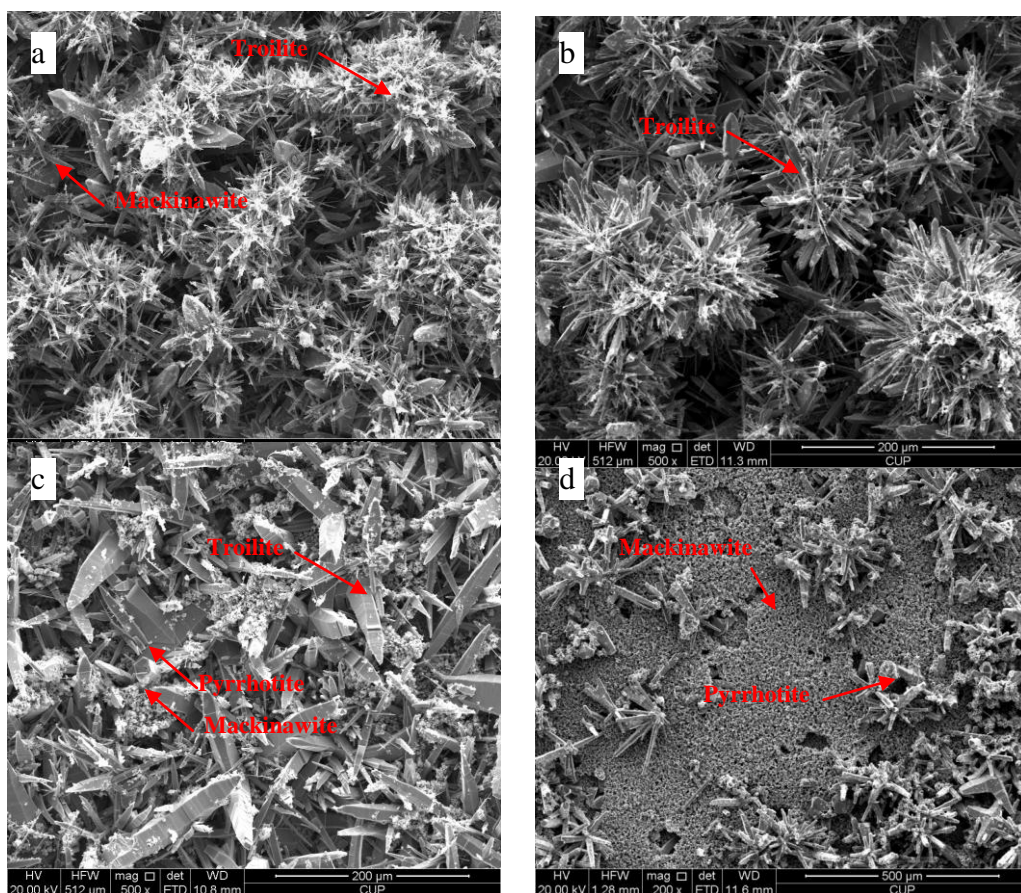
Figure 4. SEM photographs of the surface of the specimens exposed in the hydrogen permeation test to a 5% NaCl solution with 1.0 MPa H_2S at different temperatures, (a) 25°C, (b) 35°C, (c) 50°C, (d) 80.

Because the hydrogen permeation curve is significantly influenced by the corrosion product film, the corrosion films were observed using SEM, as shown in Fig. 4. The structure was discriminated using XRD, as shown in Fig. 5. The microscopic morphology of the corrosion product film formed with 1.0 MPa H_2S at 25°C is drusy and exhibited massive grains, as shown in Fig. 4a. The

results of the XRD measurements show that the corrosion products consisted of a mixture of troilite (hexagonal FeS) and mackinawite (tetragonal FeS), as shown in Fig. 4a. The drusy and acicular grains are easily distinguished to be troilite and the massive grains are mackinawite.
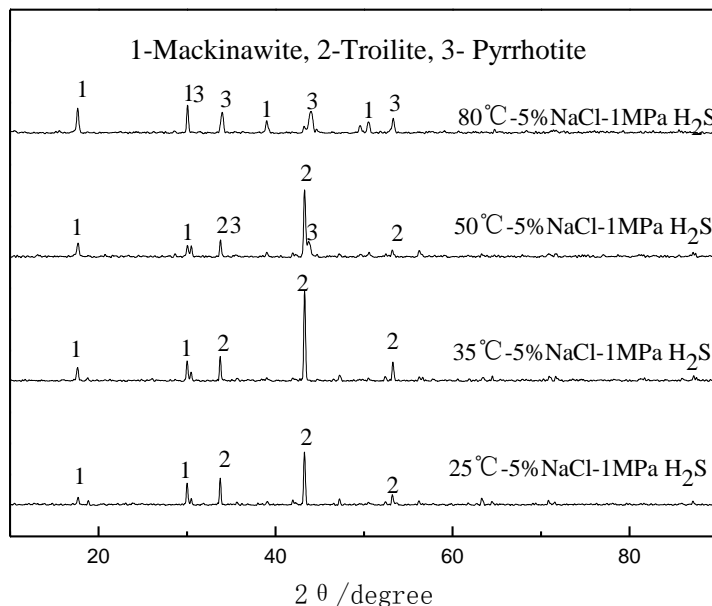

Figure 5. XRD patterns for the corrosion films formed on the permeation specimens.

When the temperature increased to 35°C, the drusy grains increase in size, but the component, which also consisted of the mixture of troilite and mackinawite, did not change significantly (Fig. 4b). However, when the temperature increased to 50°C, the microscopic morphology of the corrosion product film exhibited little change and exhibited a type of randomly distributed crystalline grains. The XRD analysis indicates that the corrosion products consisted of a mixture of acicular troilite, flaky mackinawite and a spot of prismatic pyrrhotite (Fig. 4c and 5). When the temperature increased to 80°C, the microscopic morphology of the corrosion product film obviously changed and exhibited drusy and prismatic grains growing from granular gains (Fig. 4d). The XRD analysis indicates that the corrosion products consisted of the mixture of mackinawite (granular gains) and pyrrhotite (drusy and prismatic grains). The analysis of the SEM and XRD data indicates that the structure of the corrosion film changed from the mixture of troilite and mackinawite to the mixture of mackinawite and pyrrhotite as the temperature increased from 25°C to 80°C in the environment containing 1.0 MPa H_2S. All of the structures can provide protection by inhibiting the production of hydrogen atoms, but the corrosion films formed at higher temperature exhibited more protective properties. The enhanced protection suggests that the metastable mackinawite can convert into troilite and pyrrhotite, and the latter exhibits greater stability, more rapid growth and more protective properties. The analytic results are in accordance with the hydrogen permeation curves and the values of the solubility as described above.

3.2 Corrosion rate test

The average corrosion rates (CR) of L360NCS steel in the H_2S-containing solutions at different temperatures were obtained from the weight loss tests. Fig. 6 shows the results of the average CR at different temperatures.
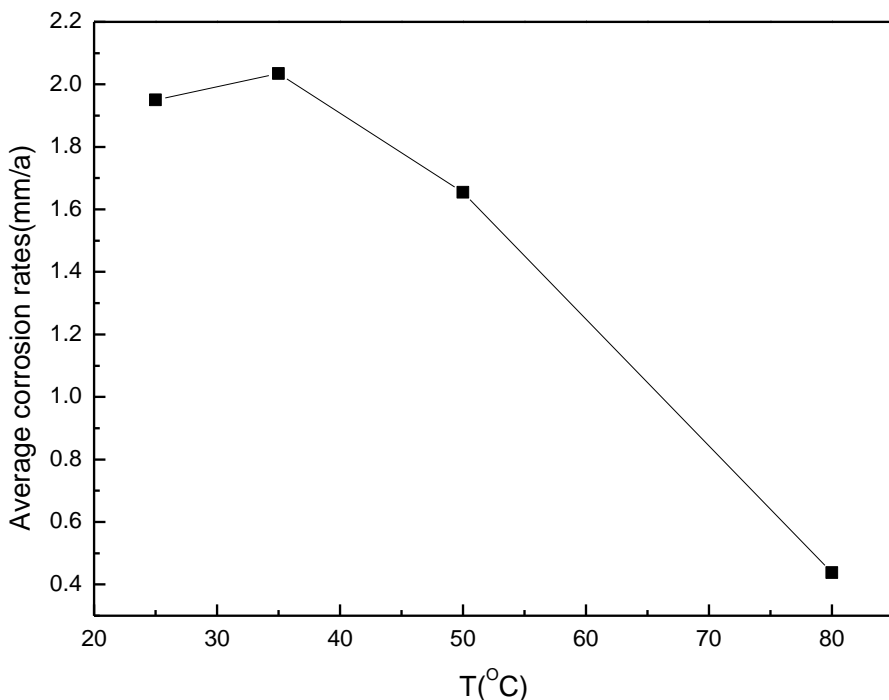
Figure 6. The corrosion rate of L360NCS pipeline steel in the environments composed of 5%NaCl solution with 1.0 MPa H_2S at different temperatures.

The result from Fig. 6 indicates that the average corrosion rates are very high for the four temperature points compared with the criterion of average corrosion rates (NACE RP-0775-91) that are considered when the average corrosion rate is over 0.125 mm/a and the pipeline steels are subject to serious corrosion. Under these conditions, the CR of the samples at 25°C and 35°C are obvious higher than others. While over 35°C, the CR decreased gradually. The trend of CR is similar to that of the total hydrogen permeation flux. Both the CR and the total hydrogen permeation flux indicate the occurrence of steel damage in the H_2S environment. When the test conditions are favourable for the formation of different types of protective iron sulphide films, higher temperature may help facilitate the film formation. Depending on whether the solubility of protective films is exceeded, temperature can either increase or decrease the corrosion rate. In the case of corrosion where protective corrosion films do not form (typically at low pH and low partial pressure H_2S), the corrosion rate increases with increasing temperature. However, when the protective corrosion films are exceeded, increased temperature will accelerate the kinetics of precipitation and facilitate the formation of protective corrosion films, thus decreasing the corrosion rate.

4. CONCLUSIONS

The hydrogen permeation and corrosion rate test for L360NCS pipeline steel have been performed at different temperatures in a 5% NaCl solution with 1.0 MPa H_2S. The following conclusions can thus be drawn:

(1)   All of the hydrogen permeation curves exhibited three stages: rising stage, declining stage and steady stage. The peak values of the hydrogen permeation curves increased as the temperature increased from 25°C to 80°C.

(2)   The mean value of the hydrogen diffusivity increased with increasing temperature. The peak values of hydrogen solubility of the specimens initially increased and then decreased and have a maximum value at 50°C, but the total hydrogen permeation flux before the steady stage decreased with increasing temperature and the hydrogen ion concentration did not change significantly.

(3)   The crystal structure of the corrosion product films formed on the specimen surface converted from a mixture of troilite (hexagonal FeS) and mackinawite (tetragonal FeS) to a mixture of mackinawite (granular gains) and pyrrhotite (drusy grains). The latter exhibits better protective properties.

(4)   The average corrosion rates of the samples at 25°C and 35°C are obviously higher than the others, while over 35°C, the CR decreased gradually. The trend of CR is similar to that of the total hydrogen permeation flux.

References

1. S. Zheng, C. Li and C. Chen, *Metallofiz. Nov. Tekh+.*, 34 (2012) 57.
2. A. Barnoush and H. Vehoff, *Acta Mater.*, 58 (2010)5274.
3. W. Chu, Y. Wang and L. Qiao, *J. Nucl. Mater.*, 280 (2000)250.
4. N. Moody, M. Baskes, S. Robinson and M. Perra, *Eng. Fract. Mech.*, 68(2001)731.
5. K. Splichal, J. Berka, J. Burda and M. Falcník, *Int. J. Pres. Ves. Pip.*, 89(2012)42.
6. J. Xia, A. Kamps, B. Rumpf and G. Maurer, *Fluid Phase Equilibr.*, 167(2000)263.
7. S. Fujimoto and H. Tsuchiya, *Corros. Sci.*, 49(2007)195.
8. J. Tang, Y. Shao, J. Guo, T. Zhang, G. Meng and F. Wang, *Corros. Sci.*, 52(2010)2050.
9. H. Ma, X. Cheng, G. Li, S. Chen and Z. Quan, *Corros. Sci.*, 42(2000)1669.
10. C. Ren, D. Li, Z. Bai and T. Li, *Mater. Chem. Phys.*, 93(2005)305.
11. H. Ma, X. Cheng, S. Chen, C. Wang, J. Zhang and H. Yang, *J. Electroanal. Chem.*, 45(1998)111.
12. I. Kabulska, J. Flis, T. Zakroczymski, *Electrochim. Acta.*, 53(2008)3094.
13. J. Catalano, M.G. Baschetti and G. Sarti, *Int. J. Hydrogen Energ.*, 36(2011)8658.
14. L. Tsay, M. Chi, Y. Wu, J. Wu and D. Lin, *Corros. Sci.*, 48(2006)1926.
15. C. Gabrielli, G. Maurin, L. Mirkova, H. Perrot and B. Tribollet, *J. Electroanal. Chem.*, 590(2006)1.
16. W. Luu, P. Liu and J. Wu, *Corros. Sci.*, 44(2002)1783.
17. T. Zakroczymski and E. Owczarek, *Acta Mater.*, 50(2002)2701.
18. C. Zhou, S. Zheng, C. Chen and G. Lu, *Corros. Sci.* 67(2012)184.

19. M. Burgess and R. Germann, *Aiche J.*, 15(1969)272.
20. M. Devnathan and Z. Stachurski, *J. Electrochem. Soc.*, 111(1963)619.
21. O. Suleimenov and R. Krupp, *Geochim. Cosmochim. Acta*, 58(1994)2433.
22. A. Ellis and W. Giggenbach, *Geochim. Cosmochim. Acta*, 35(1971)247.